ESTIMATION OF SEISMIC HAZARD FOR KATHMANDU, NEPAL AND ADJACENT REGIONS

by

Chenna Rajaram, Neelima Patnala VS, Pradeep Kumar Ramancharla

in

17th World Conference on Earthquake Engineering,
: 1
-12

Japan

Report No: IIIT/TR/2020/-1

Centre for Earthquake Engineering
International Institute of Information Technology
Hyderabad - 500 032, INDIA
September 2020

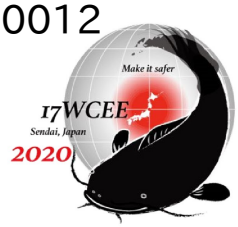

17th World Conference on Earthquake Engineering, 17WCEE
Sendai, Japan - September 13th to 18th 2020

ESTIMATION OF SEISMIC HAZARD FOR KATHMANDU, NEPAL AND ADJACENT REGIONS

C. Rajaram[(1)], P. Neelima[(2)], R. Pradeep Kumar[(3)]

[(1)] *Assistant Professor of Civil Engineering, Rajeev Gandhi Memorial College of Engineering and Technology, Nandyal, 518 501, INDIA, drchenna78@gmail.com*
[(2)] *Doctoral Student, Earthquake Engineering Research Centre, International Institute of Information Technology, Hyderabad, 500 032, INDIA, vspatnala.neelima@research.iiit.ac.in*
[(3)] *Professor of Civil Engineering, Earthquake Engineering Research Centre, International Institute of Information Technology, Hyderabad, 500 032, INDIA, ramancharla@iiit.ac.in*

Abstract

An earthquake Mw7.8 occurred on 25 April 2015 in a seismically dominant area of Nepal. No major earthquakes (>Mw7.0) were recorded in the past two decades, though Nepal is one of the active seismic regions in the world. The combined effect of the main event and the aftershocks, which are temporally distributed over 40 days, has led to a huge devastation, killing thousands of people in the epi-central area. A complete seismic catalog and influencing parameters such as type of fault, epi-central/hypo-central distance, type of soil are required for a region to assess seismic hazard scenario. The seismic hazard can be represented in terms of Peak Ground Acceleration (PGA), which is the most widely used parameter in strong motion studies.

The main objective of this paper is to understand the characteristics of ground motion of the 2015 Nepal earthquake. Since the available ground motion records are limited, an attempt has been made to generate ground motion records using a modified semi-empirical approach. Contour maps of PGA and intensity have also been generated. It is observed that around 22% of buildings experienced an intensity of VI on MMI scale at Bageswari mandal. A few buildings have experienced an intensity of VII in Thankot, Seuchatar, Satikhel, Mahadevathan, Indrayani, Chhaimale, and Balambu.

Keywords: Peak Ground Acceleration; Intensity; Seismic Hazard

1. Introduction

The Mw7.8 earthquake struck Nepal on 25 April 2015 at 06:11:26 hours UTC. The epicenter of the earthquake was located at 28.147°N 84.708°E, which is about 35 km towards ESE of Lamjung, Nepal, at a shallow depth of 15 km. The major aftershock ML6.9 occurred on 26 April 2015 in the same region with an epicenter located about 17 km south of Kodari, Nepal (Dilli Ram Thapa et al., 2018). The death toll from this earthquake was about 9000 (source: Whitney et.al., 2017). Apart from Nepal, other countries like India, China and Bangladesh were also affected by the earthquake. Significant damage has been observed to old structures in Bhaktapur, Patan, Kapan, Sakhu, Gogabu, and Balaju. However, most of the reinforced concrete frame structures did not experience major damage in Nagarjun (Source: Geotechnical Extreme Event Reconnaissance (GEER Report)).

The 2015 Nepal earthquake occurred due to the continental collision between Indian and Eurasian plates, which are converging at a relative rate of 40-50 mm/yr. Due to northward thrusting of Indian plate under Eurasian plate, numerous earthquakes generate which makes the Himalayan region seismically active. Several active faults came up during the collision process of the Indian and the Eurasian plates in the Himalaya region, namely, the Main Central Thrust (MCT), the Main Boundary Thrust (MBT), the Himalayan Frontal Thrust (HFT), the Main Karakuram Thrust (MKT) and the Main Mantle Thrust (MMT) shown in figure 1. The 2015 Nepal earthquake has occurred in between MCT and MBT due to thrust faults in the Himalaya region. The rupture plane of the 2015 Nepal earthquake strikes parallel to the Himalayan Belt WNW to ESE, and dips with 11° to the North. The rupture duration and relative slip range between 45-60 seconds and 4-5 m. The estimated length, slip and rupture duration of the earthquake fault for a moment

magnitude of 7.8 are 132 km, 6 m and 67 seconds from the empirical relations developed by Aydan (2007), respectively. The 1934 Nepal earthquake Mw8.0 had produced a surface rupture of 5-7 m displacement, which was one of the largest earthquakes in Nepal (Sapkota et al., 2013).

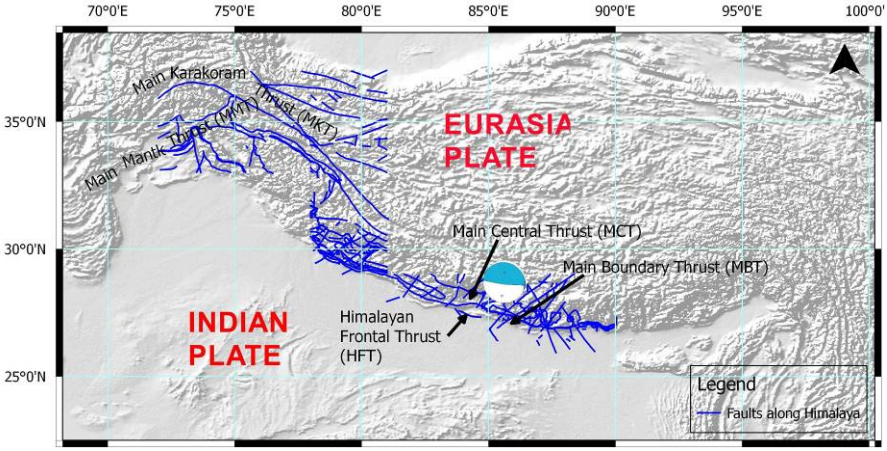

Figure 1. Location of MKT, MMT, HFT, MCT and MBT faults along Himalaya and presence of MCT, HFT, and MBT in Nepal.

Most of the earthquakes in Nepal are shallow focus earthquakes. The seismicity of Nepal with respect to magnitude and depth is shown in figure 2. A foreshock of M4.1 occurred immediately preceding the main event. Four events of magnitude M6 or larger magnitude have occurred within 250 km from the epicenter of the 2015 Nepal earthquake (Source: National Seismological Center (NSC), Nepal). Around 460 aftershocks occurred after the 2015 Nepal earthquake with local magnitude of $M_L \geq 4.0$ as of 30 June 2015 shown in figure 3 (Source: NSC, Nepal). Severe damage took place in Kathmandu during the 2015 Nepal earthquake due to (a) distribution of aftershocks extended up to 130 km to the east of the epicenter and (b) the rupture propagated from west to east. Most of the aftershocks were at the relatively shallow depth of less than 15 km below the Earth's surface.

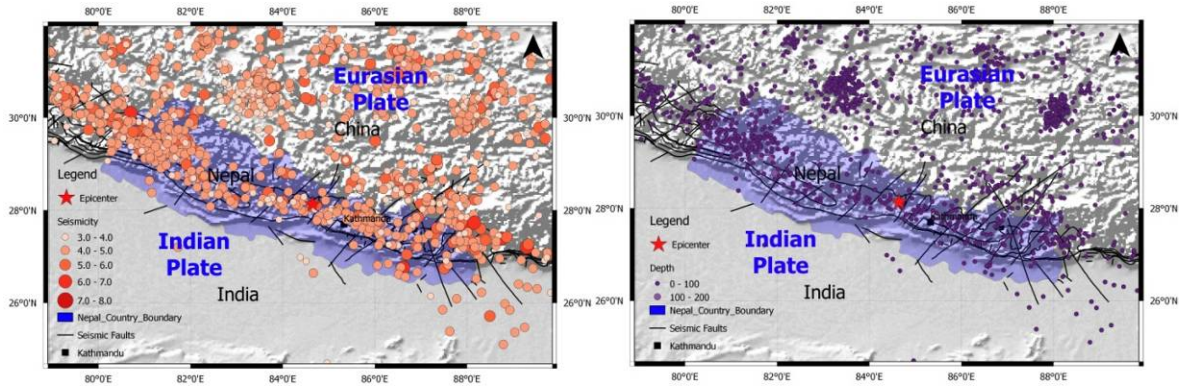

(a) Magnitude (b) Depth in km

Figure 2. Seismicity of Nepal since 1898 to 2013 with respect to (a) magnitude and (b) depth (Data source: USGS).

2. Review of Past Earthquakes in Himalayan Region

Past studies found that over two-third of the accumulated strain energy still remains to be released in the entire 2200 km long and 100 km wide Himalayan locked zone which is formed due to the brittle and colder surface above the locking line at the collision of Indian and Tibet underneath the lesser Himalayas in Nepal (Mitra et al., 2015). This excess stored energy is capable of producing a few great earthquakes in the Himalayas (Bilham et al., 2005). The 1555 Kashmir (Mw7.6), 1803 Kumaon (Mw8.1), 1833 Nepal earthquake (Mw7.7) and 1905 Kangra earthquake (Mw7.8) indicate that the rupture lengths were less than 120 km. But, the 1934 Bihar-Nepal (Mw8.1) earthquake caused rupture of 200-300 km long segment (Sapkota et al., 2013; Bollinger et al., 2014).

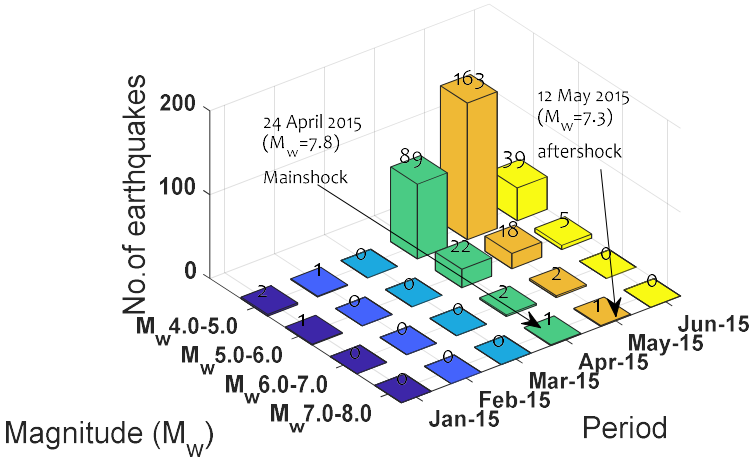

Figure 3. Distribution of foreshocks and aftershocks of the 2015 Nepal earthquake from 01January2015 to 30 June 2015 (Data source: NSC, Nepal).

The major earthquakes that have occurred in the Himalayan region are 1555-Kashmir (Mw7.6), 1803-Garhwal (Mw8.1), 1833-Nepal (Mw7.7), 1869-Kathmandu (Mw7.4), 1885-Kashmir (Mw6.4), 1897-Assam (Mw8.0), 1905-Kangra (Mw7.8), 1916-Mahakali (Mw7.3) zone, 1934-Bihar-Nepal (Mw8.1), 1966-Nepal-India (Mw6.0), 1980-Pithoragarh (Mw6.5), 1988-Nepal (Mw6.9), 2005-Kashmir (Mw7.6), 2011-Sikkim (Mw6.9) and the recent 2015 Nepal (Mw7.8) earthquake. These great earthquakes that occurred along the Himalaya destroyed vast regions (Bilham et al., 2001). Numerous studies have been done on past great earthquakes in the Himalayan region. In central Nepal, historical earthquakes in Kathmandu in 1408, 1681, 1767, 1808, 1826, and 1866 had insufficient information about rupture zones (Martin et al., 2015). The geologists are concerned about paleo-seismic investigations across the Himalaya. A slip value of 4 m and 8 m were observed in 1934 Bihar-Nepal earthquake and 1950 Assam earthquake, respectively (Bilham et al., 2001). The occurrence of the new earthquakes indicates that the rigor to paleo-seismological research is required to be increased to provide information about the future earthquakes. The active faults in the country are mainly due to the southern front of the mountains. From the studies carried out at the trench near Khemalpur village, Mahara Khola and Mohana Khola of Nepal, it is identified that two locations are likely places for the future earthquakes that can be categorized into the potential seismic gaps (Upriti et al., 2007).

A peak slip of 4.48 m was observed along the fault plane of length 160 km and width 160 km during the 2015 Nepal earthquake (Source: USGS; Mitra et al., 2015). The rupture parameters from the 2015 Nepal earthquake are constrained by finite fault modeling (Hayes et al., 2015). The earthquake was also recorded by several high-rate continuous Global Positioning System (GPS) receivers (time interval (Δt) = 0.2 s) above and near the rupture area (Galetzka et al., 2015; Grandin et al., 2015). The mainshock event gave rise to ground motions with a predominant period of 5 s provides an explanation for low intensities (Dixit et al., 2015; Galetzka et al., 2015). The predominant periods of large aftershocks of the 2015 Nepal earthquake, including the M7.3 event on 12 May 2015, were lower than that of the mainshock and more consistent with the expected predominant period of the basin response (Dixit et al., 2015). The rupture speed of 2015 Nepal earthquake was ~1.0 km/s for first 20 s and then accelerated to ~3.0 km/s for the remaining 30-40 s (Wang et al., 2016). The slip and the slip velocity resulted in a wide variety of ground motions at different locations from the fault plane. These ground motions are required to estimate the spatial and temporal variation of the ground movement that has taken place in and around the region. The spatial distribution of variation of ground motion parameters is useful in damage assessment of the structures in the region. In contrast to the need of the spatial distribution of the ground motions, the present earthquake was recorded at few stations, for which the ground motion data is available. To fulfill the purpose of estimating ground motions, a study has been conducted to generate ground motions of the 2015 Nepal earthquake at 4 stations using modified semi-empirical approach. The same approach has been validated with the 1991 Uttarkashi earthquake. Also, the intensities of the 2015 Nepal earthquake have been estimated. Later, the analysis has been extended to

estimate hazard scenario at each mandal of Kathmandu, Bilaspur, and Lalitpur districts. The description of modified semi-empirical approach is as follows.

3. Methodology to Generate Ground Motion

The following section briefly describes the procedure to generate synthetic accelerogram. The semi-empirical simulation technique is based on ω^2 model. In the composite source method, synthetic accelerograms were generated using wave propagation theory for 1991 Uttarkashi earthquake (Yu et al., 1995). This method has proved to be quite successful to generate synthetic accelerogram. However, it requires lot of geophysical parameters (fault plane solutions, stress drop etc.), which are always easily unavailable for a site of interest. On the other hand, empirical Green's function method has advantage that it doesn't require computation of propagation and local site effects. This method is only applicable where ground motion records of small events exist in the area of study. Unfortunately, it is rare to have those records for a site of interest. In stochastic simulation method, the source is assumed as a point. But this method fails at near source region of large earthquakes. The effect of large finite source can significantly influence the characteristics of ground motion. A similar approach is arrived to model these effects to subdivide the large fault into smaller parts, in which each sub-fault is treated as point source. The ground motion obtained at the site is contribution of all sub-faults.

Semi-empirical method has advantages such as i) it does not require aftershock records at the site of simulation which is necessary in empirical Green's function method, ii) detailed velocity structure is not required, iii) and the fault plane solution as in the case of the composite source model. The aftershock records and velocity structure are unavailable for the event. With these advantages, the authors have chosen semi-empirical approach is a better choice for generating synthetic ground motions for the Nepal earthquake. The semi-empirical simulation method is as follows:

In the stochastic simulation technique, the normalized white Gaussian noise of zero expected mean and variance has been chosen of desired length. The shape of acceleration spectra A(f) at a site located at a hypo-central distance R is as follows

$$A(f) = \mathrm{CS(f)P(f)}\left[e^{(-\pi \mathrm{fR}/\beta \mathrm{Q})} / R\right] \tag{1}$$

Where C is a constant scaling factor including seismic moment (Mo) given by Boore (1983). The filter S(f) represents the source acceleration spectrum defined by Brune (1970), filter P(f) represents attenuation of high frequencies as used in Boore (1983), R is hypo-central distance from source to site in km, β is shear wave velocity in km/sec and Q is a frequency dependent quality factor.

$$S(f) = \frac{(2\pi \mathrm{f})^2}{\left[1+\left(\mathrm{f}/\mathrm{f_c}\right)^2\right]};\ P(f) = \frac{1}{\left[1+\left(\mathrm{f}/\mathrm{f_m}\right)^8\right]^{0.5}}. \tag{2}$$

Where fc is the corner frequency and fm represents high frequency cutoff range of the high-cut filter. The corner and maximum frequencies are calculated as follows:

$$f_c = 4.9\mathrm{x}10^6 \beta(\Delta\sigma / M_o)^{1/3};\ \mathrm{f_m} = 7.31\mathrm{x}10^3 \mathrm{M_o}^{-0.12}. \tag{3}$$

Where Δσ is stress drop in bars, Mo is seismic moment of an earthquake in dyne.cm. The acceleration spectrum in frequency domain is converted into time domain. However, time domain representation of acceleration ground motion record overestimates the high frequency and underestimates the low frequency in synthetic ground motion. This is due to difference in duration of slip of the target and small earthquake considered as sub-faults. A correction function F(t) is given by Irikura et al., (1983, 1997) is as follows:

$$F(t) = \delta(t) + [(N-1)/T_R(1-e^{-1})].e^{(-t/T_R)}. \quad (4)$$

Where δ(t) represents delta function, N is the total number of sub-faults along the length or width of the rupture plane and TR is the rise time of the target earthquake. The acceleration record $A_{ij}(t)$ is as follows:

$$A_{ij}(t) = F(t).a_{ij}(t). \quad (5)$$

Where i and j represent the position of sub-fault along length and width of fault plane respectively, a_{ij} is empirical relation of peak ground acceleration. The seismological parameters for Nepal earthquake are shown in table 1. Further, the acceleration envelope waveform $e_{ij}(t)$ is determined by Kameda and Sugito (1978).

$$e_{ij}(t) = T_{ss}\left[a_{ij}\frac{t}{T_d}e^{\left(1-\frac{t}{T_d}\right)}\right]; \quad \mathrm{E(t)} = \sqrt{\sum_{i=1}^{N}\sum_{j=1}^{N} e_{ij}^2(t-t_{ij})}. \quad (6)$$

Where a_{ij} is empirical relation of peak ground acceleration and is shown in table 1 (Patnala et al, 2017).

Table 1. Seismological parameters used for generating synthetic accelerogram of 2015 Nepal earthquake

Parameters	Values
Magnitude	7.8
Type of fault	Thrust fault
Shear Wave Velocity, β (km/sec)	3.2
Rupture Velocity, V_r (km/sec)	2.8
Seismic Moment, M_o (dyne.cm)	$8.056x10^{27}$ (Dhanya et al., 2016)
Frequency dependent Quality factor	$Q(f)=253f^{0.8}$(Dhanya et al., 2016)
Stress Drop, Δσ (bar)	74 (Dhanya et al., 2016)
Maximum frequency (f_{max})	$7.31x10^3\ M_o^{(-0.12)}$
Time interval (s)	0.02
Attenuation: $\log_{10}(a) = 1.168+0.288M-0.65\log_{10}\sqrt{(R^2+h^2)}+0.009S+0.443$ (Source: Patnala et al, 2016)	
Corner frequency (f_o)	$4.9x10^6\ \beta(\Delta\sigma/M_o)^{0.33}$

The parameters required to define the model of the rupture plane are its length (L), width (W), length and width of the sub-faults (Le, We), nucleation point, strike (φ) and dip (θ) of rupture plane, rupture velocity (Vr) and shear wave velocity (Vs) in the medium. The rectangular rupture plane of a target earthquake is divided into NxN sub faults. The acceleration record $ac_{ij}(t)$, released from different sub faults reaches the observation point at different time. The arrival time at the observation point tij depends on the time taken by rupture from nucleation point to ijth sub-fault with rupture velocity Vr and time taken by energy released from ijth sub fault to reach the observation point. The total time taken t_{ij} is given as (Joshi et al., 2004):

$$t_{ij} = (r_{ij}/V) + (\xi_{ij}/V_r) \quad (7)$$

Where r_{ij} is the distance from the observation point to the ijth sub fault and ξ_{ij} is the distance travelled by the rupture from nucleation point to particular sub fault. Following formula is used for obtaining horizontal component of records along the direction of strike and the direction of dip of the modeled fault, respectively, from resultant component $ac_{ij}(t)$, released by ijth sub-fault. Figure 4 shows schematic diagram of modified-empirical approach and the division of total acceleration record $ac_{ij}(t)$ into components along strike and dip directions.

$$ac_{ij}^{X}(t) = ac_{ij}(t).\cos\theta_{ij}.\cos\phi_{ij};\quad ac_{ij}^{Y}(t) = ac_{ij}(t).\cos\theta_{ij}.\sin\phi_{ij}. \tag{8}$$

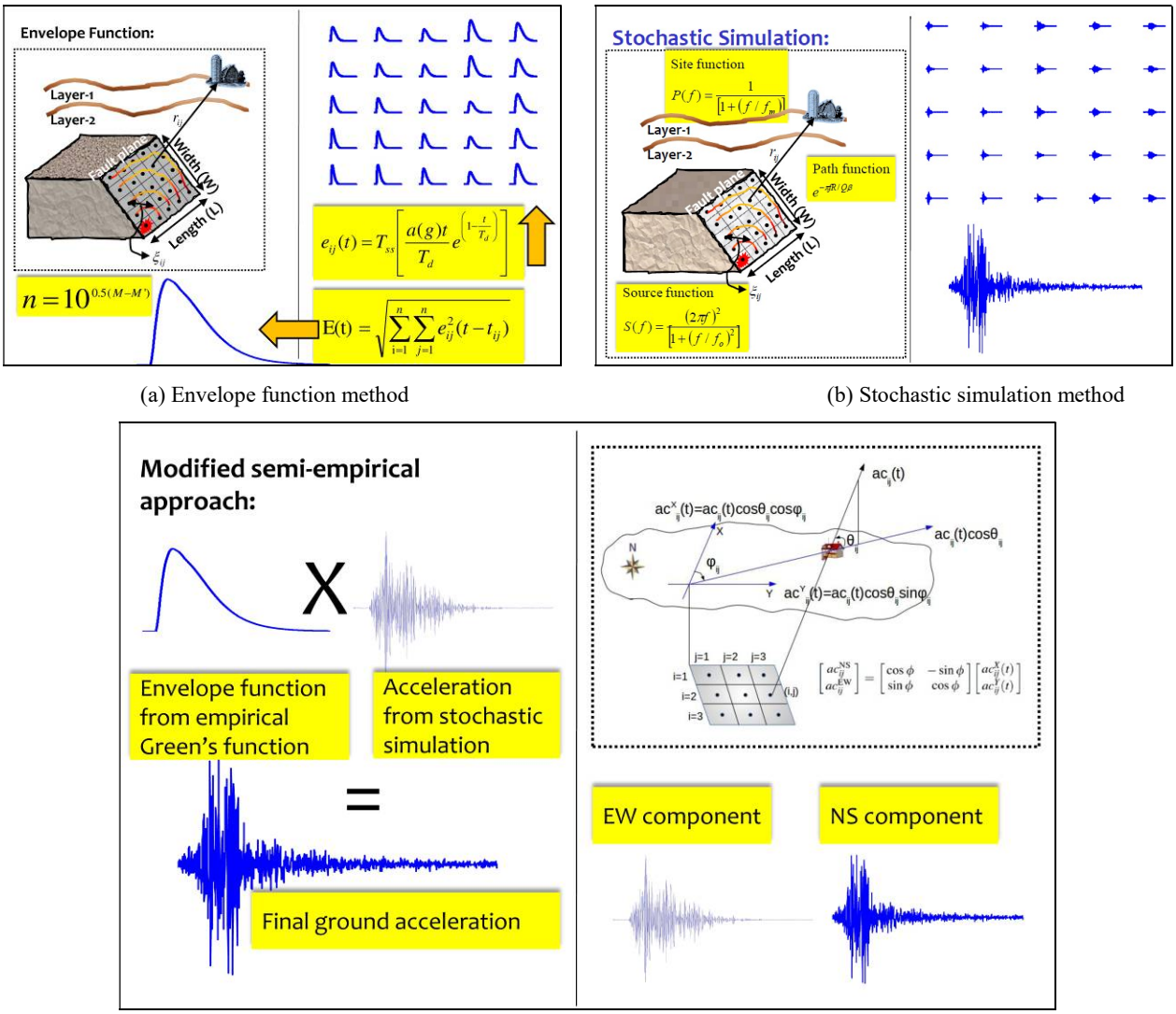

(a) Envelope function method

(b) Stochastic simulation method

(c) Modified semi-empirical method

Figure 4. Schematic diagram of (a) Envelope function method, (b) Stochastic simulation method and (c) modified semi-empirical approach (Rajaram et al., 2016)

4. Validation

The above method is quite successful to generate strong ground motions for a wide range of earthquakes like 1991 Uttarkashi earthquake (Joshi et al., 2001), 1999 Chi-Chi earthquake (Rajaram et al., 2014), 2011 Sikkim earthquake, 2011 Tohoku earthquake (Joshi et al., 2012, 2014), 2013 Doda earthquake (Rajaram et al., 2016) and 2013 Iran-Pakistan border earthquake (Rajaram et al., 2014). Also, the ground motion records are compared to Stochastic Finite Fault Simulation method and Stochastic Point Source method to validate the modified semi-empirical approach (Rajaram et al., 2016). Based on above study, it is concluded that the modified semi-empirical approach yields satisfactory results. The effect of synthetic accelerogram due to asperities and different soil layers have not considered in this study. A MATLAB code is written to obtain synthetic ground motions. Ground acceleration records have been simulated for 1991 Uttarkashi earthquake at Uttarkashi station, which is located 25 km from the source of the earthquake. The parameters used for generating ground motions of the 1991 Uttarkashi earthquake are tabulated in table 2. The peak ground

acceleration recorded at the station is 3.04 m/s^2 and 2.37 m/s^2 along fault parallel (FP) and fault normal (FN) components respectively. The PGA obtained using modified semi empirical approach at Uttarkashi station along FN and FP were 3.24 m/s^2 and 1.8 m/s^2 respectively. The results are satisfactorily good along FP component and fairly good along FN component shown in figure 5. The variation of response spectra between observed and simulated along FN component is higher than FP component shown in figure 5. The results are fairly good at time periods longer than 1.5 s (Rajaram et al., 2016). From the above study, it is concluded that the modified semi-empirical approach yields satisfactory results. Hence, the same methodology is used to generate ground motions for the 2015 Nepal earthquake.

Table 2. Seismological parameters used for generating synthetic accelerogram of 1991 Uttarkashi earthquake

Parameters	Values
Magnitude	7.0
Type of fault	Thrust fault
Shear Wave Velocity, β (km/sec)	3.2
Rupture Velocity, V_r (km/sec)	2.8
Seismic Moment, M_o (dyne.cm)	$1.8x10^{26}$ (Joshi et al., 2001; Ashish et al., 2012)
Frequency dependent Quality factor	$Q(f)=140f^{1.018}$(Ashish et al., 2012)
Stress Drop, Δσ (bar)	33 (Ashish et al., 2012)
Maximum frequency (f_{max})	$7.31x10^3$ $M_o^{(-0.12)}$
Time interval (s)	0.02
Attenuation: $\log_{10}(a) = -0.62+0.177M-0.982 \log_{10}(R+e^{0.284M})+0.132F-0.0008ER$ (Source: Joshi et al, 2001)	
Corner frequency (f_o)	$4.9x10^6$ $\beta(\Delta\sigma/M_o)^{0.33}$

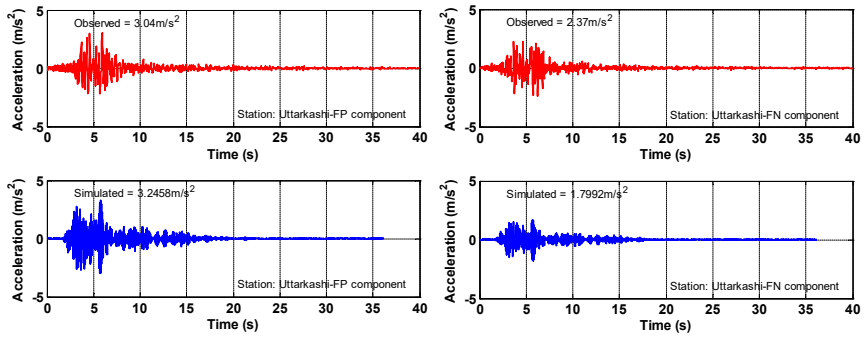

(a) Observed and simulated ground acceleration time history records

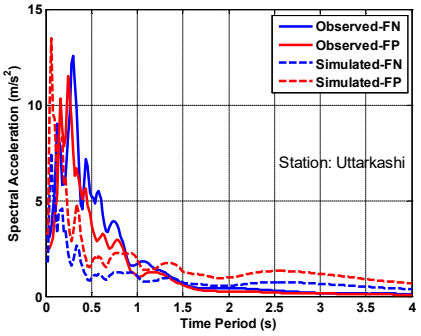

(b) Response spectra

Figure 5. Observed and simulated accelerograms and response spectra of the 1991 Uttarkashi earthquake at Uttarkashi station.

5. Generation of Ground Motions

Observed Ground Motions

The main event of the 2015 Nepal earthquake was recorded at 4 seismic stations, namely KTP (Kirtipur Municipality Office, Kirtipur), TVU (Central Department of Geology, Tribhuvan University, Kirtipur), PTN (Pulchowk Campus, Institute of Engineering, Tribhuvan University, Patan), and THM (University Grants Commission Office, Sanothimi, Bhaktapur) (Ref: figure 6). The largest peak ground acceleration (PGA) of 0.254 g was recorded on EW component at station KTP, located on rock site. The PGA 0.2 g at KATNP station is considerably less than the expected value of about 0.4 g (Somerville, 2015). The horizontal PGA values were compared with earlier studies and found that the observed PGA values were smaller than those estimated by the GMPE of Patnala et al., 2016 and higher than Ahmad et al., 2016. The PGA values obtained from GMPEs of previous studies are shown in table 3. Since Kathmandu station is located on lakebed sediments of 700 m thick, the sediments would tend to amplify the ground motion. It was also noted that the

ground acceleration record at Kathmandu was dominated by the long-period waves having a period of about 4.5 s (Takai et al., 2016). The stations located on sedimentary sites (TVU, PTN, and THM) had long-period oscillations. On other hand, the vertical accelerograms had short-period oscillations at all sites. The acceleration time history records of the above stations are shown in figure 7.

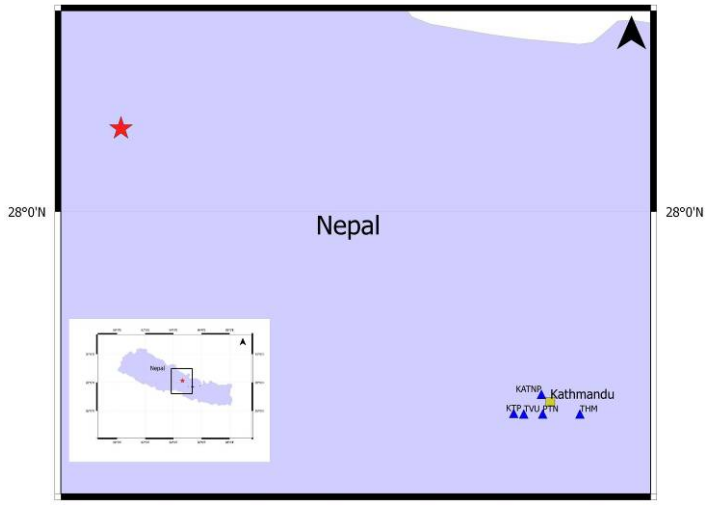

Figure 6. Location of epicenter of the 2015 Nepal earthquake is represented with red star. The location of seismic stations is represented with triangles.

Table 3. Comparison of PGA values of the 2015 Nepal earthquake at four stations from past studies.

Station	Co.ordinates		Epicentral Distance (km)	*Patnala et al., 2016 (g)	**Ahmad et al., 2016 (g)	***Recorded (g)
	Latitude (^{0}N)	Longitude (^{0}E)				
KTP	27.682	85.272	80.40	0.374	0.150	0.295
TVU	27.681	85.288	81.84	0.379	0.146	0.303
PTN	27.681	85.318	84.43	0.374	0.141	0.197
THM	27.681	85.377	89.68	0.363	0.132	0.200

* - The maximum value of two horizontal components is used.
** - Single PGA value is used.
*** - Square Root of Sum of Squares of two horizontal components is used.

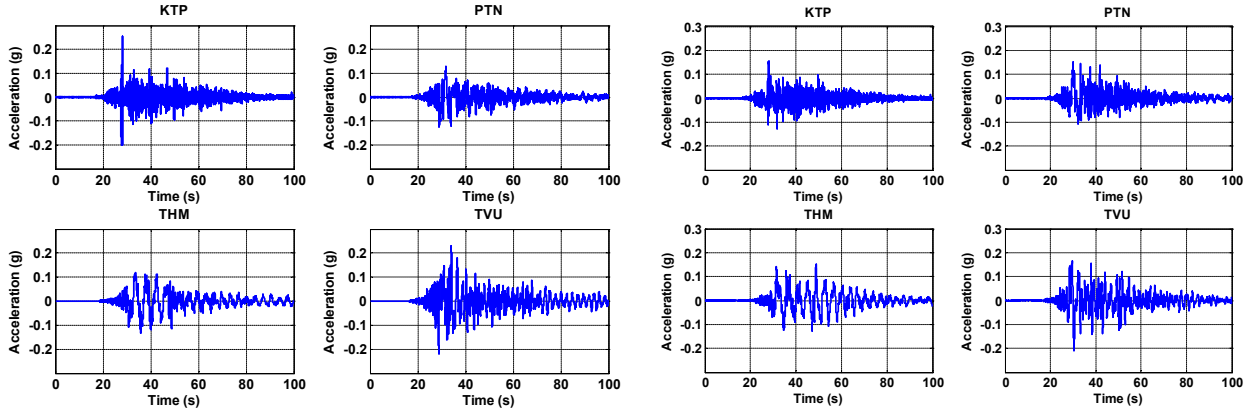

NS Component EW Component

Figure 7. Acceleration time history records at four stations along NS, and EW components.

A peak horizontal velocity of greater than 1.0 m/s was observed at TVU station. A single sided velocity pulse of 6.3 s was observed along NS component and a double sided pulse of 9.8 s was observed along EW component at KTP station. A permanent displacement of 2.28 m was observed at TVU station along EW

component. It is observed that the displacement waveforms were similar along both components at PTN and TVU stations. From Fourier amplitude spectrum, it is observed that significant drop down in the amplitude between 3.52 Hz and 5.0 Hz in NS component of Fourier spectrum. Similar pattern is observed between 3.0 Hz and 4.0 Hz in EW component respectively. It means lower frequencies are more predominant in the spectrum. The Fourier spectra at all stations along EW and NS components are shown in figure 8. The elastic acceleration response spectra at all stations along NS and EW components are shown in figure 9. Low spectral accelerations are observed at short periods (< 1 s) and high spectral accelerations are observed at long periods at Tribhuvan university. Similar pattern is observed at Kathmandu station, which corresponds to the fundamental period (T=4.5 s) of thick soil layer at Kathmandu Valley with 500 m as soil thickness (Bret et al., 2016). Research needs to be done on near-field ground motion. An attempt has been made on generation of ground motion at few stations using modified semi-empirical approach.

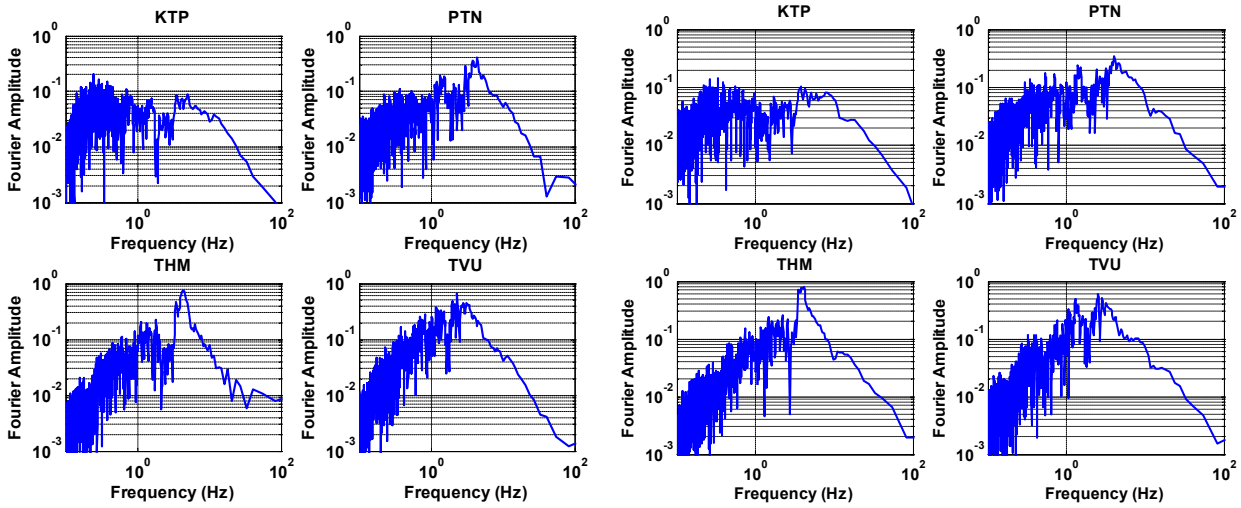

NS Component EW Component

Figure 8. Fourier amplitude spectrum at four stations along NS, and EW components (units for Fourier amplitude is in m/s^2).

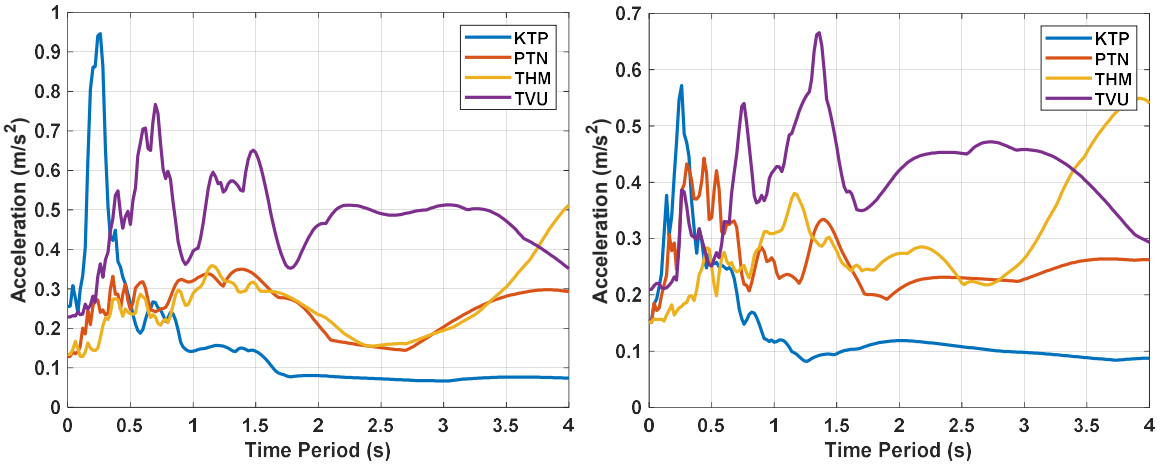

NS Component EW Component

Figure 9. Elastic acceleration response spectrum at four stations along NS, and EW components.

Simulated Ground Motions

The acceleration records are generated at KTP, PTN, THM and TVU stations along NS and EW components through modified semi-empirical approach. A comparison is made between observed and simulated ground motion values along both components and the values are shown in table 4. The station KTP is located near to the fault MBT and recorded a PGA of 0.25 g. A PGA of 0.17 g is calculated at the same station through

simulation. Acceleration time history records at four stations along NS, and EW components obtained through simulation are shown in figure 10. The simulated PGA values can be comparable with observed ground motion records at KTP, PTN and THM stations. A match of 70-90% has been observed in the PGA along EW and NS components. Since appropriate geophysical parameters are considered for preliminary analysis, long period waves are not observed in the simulation of ground motion records.

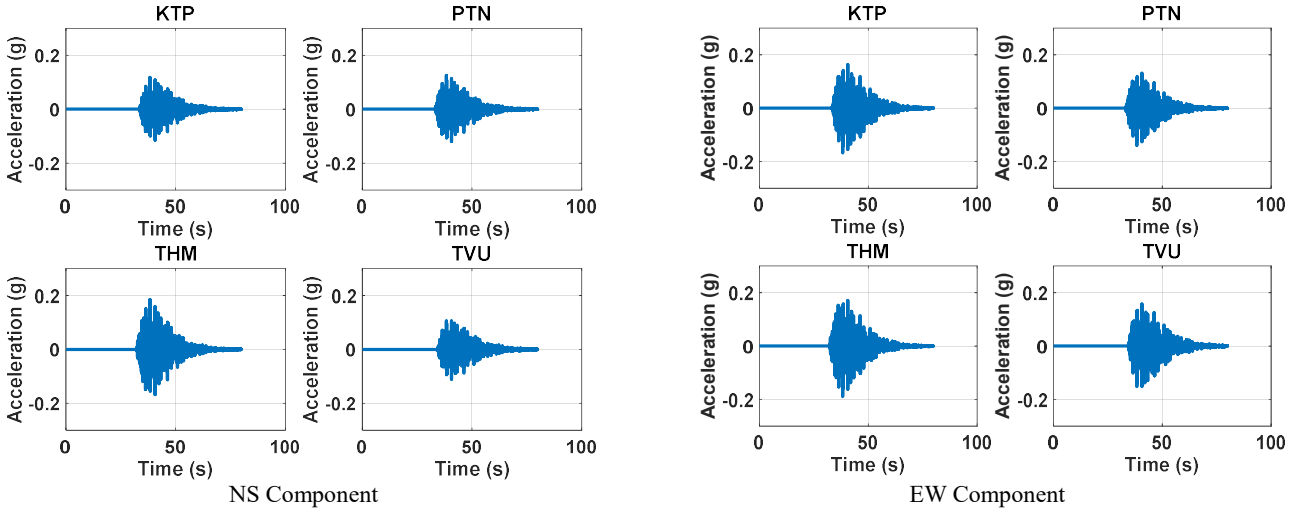

Figure 10. Acceleration time history records at four stations along NS, and EW components obtained through analytical approach.

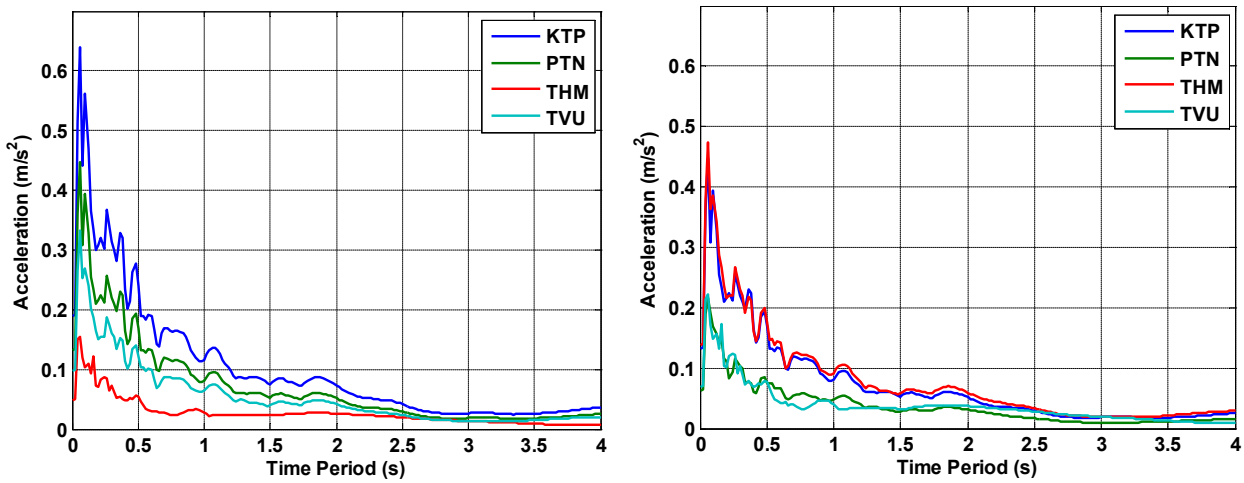

Figure 11. Elastic acceleration response spectrum at four stations along NS, and EW components through analytical approach.

Elastic acceleration response spectra have been plotted at all stations along NS and EW components shown in figure 11. The spectral amplitudes obtained from ground motion records are considerably higher at sedimentary sites (TVU, PTN and THM) than at rock sites (KTP) between periods 0.5 s and 1.5 s. Peak spectral amplitude is observed at KTP station at 0.25 s along both horizontal components. Peak spectral amplitudes are observed at period 0.1 s at all stations. The variation in simulations is due to appropriate geophysical parameters. The results can further be improved, if suitable parameters are available for Nepal region. Synthetic accelerograms are generated at all mandals of the national capital, Kathmandu and its adjacent regions Lalitpur and Bhaktapur using above method to estimate seismic hazard scenario. The geographical locations of mandals of Kathmandu, Lalitpur, and Bhaktapur and its buildings are taken from Mapcruzin (Source: http://www.mapcruzin.com/free-india-country-city-place-gis-shapefiles.htm dated 20 Jun 2018) and is shown in figure 12. The contour map is generated using GIS software and an Inverse

Distance Weighted (IDW) technique is used for interpolation between contours. The PGA contour distribution of three districts and its buildings is shown in figure 13.

Bhaktapur District: It is observed that around 22% of buildings experienced an intensity of VI on MMI scale at Bageswari mandal. Around 19% of buildings experienced an intensity of VI at Bhaktapur, located in the eastern part of Kathmandu valley. More than 60% of buildings have experienced an intensity of VI in the province of Duwakot. A few mandals (Changunarayan, Dadhikot, Jhaukhel, Kautunje, and Sirutar) have experience an intensity of VII.

Kathmandu District: Around 20% of buildings have experienced an intensity of VII in the capital city of Nepal. More than 50% of buildings experienced an intensity of VII in Chalnakhel, Chapali Bhadrakali, Dharmastali, Mahankal, Pukulachi, Ramkot, Tokha Chandeswori mandals. A few buildings have experienced an intensity of VII in Thankot, Seuchatar, Satikhel, Mahadevathan, Indrayani, Chhaimale, and Balambu.

Lalitpur District: Around 50% of buildings have experienced an intensity of VI in Jharuwarasi. Similar percentage of buildings has experienced an intensity of VII in Sainbu.

(a) Districts (b) Mandals (c) Buildings

Figure 12. (a) geographical locations of Kathmandu, Lalitpur, and Bhaktapur districts, (b) location of mandals in each district, and (c) location of buildings in each mandal

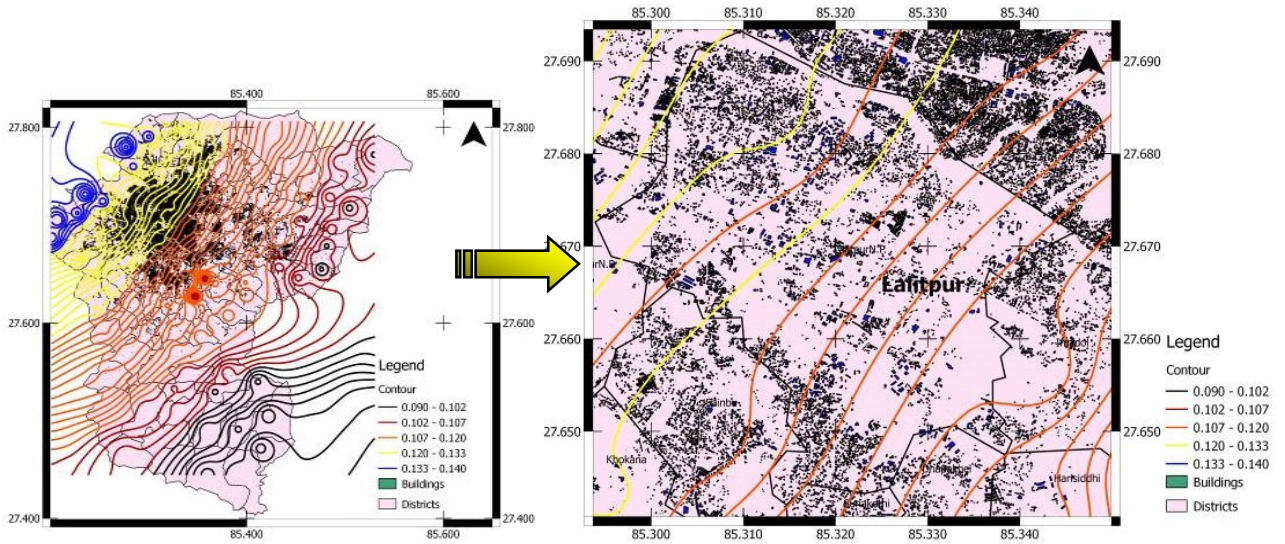

Figure 13. The PGA contour distribution of three districts and its buildings

6. Conclusions

The M 7.8 earthquake struck Nepal on 25 April 2015 at 06:11:26 hours UTC. The PGA 0.2 g is considerably less than the expected value of about 0.4 g at Kathmandu station. Since Kathmandu station is located on lakebed sediments of 700 m thick, there is a concern that these sediments would tend to amplify the ground motion. A MATLAB code has been written to generate the ground motion records at near-field seismic stations. The simulated PGA values are comparable with observed ground motion records at KTP, PTN and THM stations. A match of 70-90% has been observed in the PGA along EW and NS components. The spectral amplitudes obtained from ground motion records are considerably higher at sedimentary sites (TVU, PTN and THM) than at rock sites (KTP) between periods 0.5 s and 1.5 s. Peak spectral amplitudes are observed at period 0.1 s at all stations through analytical approach. Around 19% of buildings experienced an intensity of VI at Bhaktapur, located in the eastern part of Kathmandu valley. More than 50% of buildings experienced an intensity of VII in Chalnakhel, Chapali Bhadrakali, Dharmastali, Mahankal, Pukulachi, Ramkot, Tokha Chandeswori mandals. Around 50% of buildings have experienced an intensity of VI in Jharuwarasi. Similar percentage of buildings has experienced an intensity of VII in Sainbu.

REFERENCES

1. Ahmad R, and Singh R P (2016) “Attenuation Relation Predicted Observed Ground Motion of Gorkha Nepal Earthquake of April 25, 2015”. *Nat Haz*, 80, 311-328.
2. Aydan, O (2007) “Inference of seismic characteristics of possible earthquakes and liquefaction and landslide risks from active faults”. *The 6th National Conference on Earthquake Engineering of Turkey*, Istanbul 1, 563-574 (in Turkish).
3. Ashish H, Sharma ML (2012) “Stochastic ground-motion simulation of two Himalayan earthquakes: seismic hazard assessment perspective”. *Journal of Seismology*, 16, pp.345–369.
4. Bilham R, Vinod K. Gaur, Peter Molnar (2001), “Himalayan Seismic Hazard”, *Science* 293, 1442-1444.
5. Bilham R, (2004) “Earthquake in India and the Himalaya: Tectonics, Geodesy and History”, *Annals of Geophysics*, 47 (2), 839-858.
6. Bilham, R. and Ambraseys, N., (2005) “Apparent Himalayan slip deficit from the summation of seismic moments for Himalayan earthquakes, 1500–2000”. *Current Science*, 88(10), 1658–1663.
7. Bilham R, (2009) “The seismic Future of Cities”, *Bulletin of Earthquake Engineering*, 7 (4), 839-887.
8. Bollinger, L., Sapkota, S. N., Tapponnier, P., Klinger, Y., Rizza, M., Vander, J. W., Tiwari, D. R., Pandey, R., Bitri, A., and Berc, B., (2014) “Estimating the return times of great Himalayan earthquakes in Eastern Nepal: Evidence from the Patu and Bardibas strands of the Main Frontal Thrust”, *Journal of Geophysical Research Solid Earth* 119, 7123-7163.
9. Boore, D. M., (1983) “Stochastic simulation of high frequency ground motion based on seismological models of radiated spectra”, *Bulletin of Seismological Society America* 73, 1865-1894.
10. Bret Lizundia, Surya Narayan Shrestha, John Bevington, Rachel Davidson, Kishor Jaiswal, Ganesh Kumar Jimee, Hemant Kaushik, Hari Kumar, Jan Kupec, Judy Mitrani-Reiser, Chris Poland, Suraj Shrestha, Courtney Welton-Mitchell, Heidi Tremayne, and Maggie Ortiz (2016) “M7.8 Gorkha, Nepal Earthquake on April 25, 2015 and its Aftershocks”. *EERI Earthquake Reconnaissance Team Report*, USA.
11. Brune, J. N., (1970) “Tectonic stress and spectra of seismic shear waves from earthquakes”. *Journal of Geophysics Research* 75, 4997–5009.
12. Dhanya J, Maheshreddy G, Raghukanth S T G (2016) “Ground motion estimation during 25th April 2015 Nepal earthquake”. *Acta Geod Geophys*, 52(1), 69-93.
13. Dilli Ram Thapaa, Xiaxin Taoa, Feng Fana, and Zhengru Tao (2018) “Aftershock analysis of the 2015 Gorkha Dolakha (Central Nepal) earthquake doublet”. *Journal of Heliyon*. 4, 1-12.

